Al-doped ZnO-Coated LiNi_{1/3}Mn_{1/3}Co_{1/3}O₂ Powder Electrodes: The Effect of a Coating Layer on The Structural and Chemical Stability of The Electrode / Electrolyte Interface

Ardavan Makvandi,* Michael Wolff, Sandra Lobe, Bastian Heidrich, Martin Peterlechner, Christoph Gammer, Sven Uhlenbruck, Martin Winter, and Gerhard Wilde

LiNi_{1/3}Mn_{1/3}Co_{1/3}O₂ (NMC-111) is one of the most popular cathode materials in Li-ion batteries. However, chemical and structural instabilities of the cathode/electrolyte interface at high charge cut-off voltages cause capacity fading. Surface modifications using metal oxides are promising candidates to suppress capacity fading. Here a systematic study on the degradation mechanism of an uncoated NMC-111 powder electrode is presented. Moreover, the effect of an Al-doped ZnO (Al:ZnO) coating layer on the structural and chemical stabilities of NMC-111 electrode cycled at high charge cut-off voltages is analyzed using X-ray photoelectron spectroscopy, scanning electron microscopy and analytical transmission electron microscopy as well as electrochemical testing. The coating is applied to commercial NMC-111 powder using a microwave-assisted sol-gel synthesis method. In the case of uncoated NMC-111 electrodes, pitting corrosion due to hydrofluoric acid attacking the electrode surface, cation mixing, and an irreversible phase transformation from a trigonal layered to a rock-salt phase occurs, causing capacity fading. While, in the case of Al:ZnO – coated NMC-111 electrodes, pitting corrosion, cation mixing, and the irreversible phase transformation are mitigated. Therefore, the capacity retention and rate capability are improved as the coating layer protects the electrode surface from the direct electrolyte exposure.

1. Introduction

In the past 30 years, lithium-ion batteries (LIBs) have been extensively used as energy storage in portable electronic devices. In recent years the growing demand for LIBs development with higher energy density, cycle life, safety, and low cost as a key power source for hybrid-electric (HEVs) and electric vehicles (EVs) stimulated significant attention.[1-4] Cathode active materials (CAMs) play a significant role on the electrochemical performance of LIBs used in EVs.^[5] The layered lithium transition metal oxide LiNi_{1-x-v}Mn_vCo_vO₂ (NMC) is one of the most promising CAMs due to the cost effectiveness and high capacity compared to commercial LiCoO2 electrode. In order to obtain higher capacity and energy density, NMC CAMs should be cycled at higher charge cut-off voltages. However, the microstructural and chemical instabilities at the electrode/electrolyte interface cause capacity and voltage fading at high

A. Makvandi, M. Peterlechner, G. Wilde
Institute of Materials Physics
University of Münster
48149 Münster, Germany
E-mail: ardavan.makvandi@uni-muenster.de
M. Wolff, S. Lobe, S. Uhlenbruck
Forschungszentrum Jülich GmbH, Institute of Energy and Climate
Research, Materials Synthesis and Processing (IEK-1)
Jülich Aachen Research Alliance: JARA-Energy
52425 Jülich, Germany



The ORCID identification number(s) for the author(s) of this article can be found under https://doi.org/10.1002/admi.202300668

© 2023 The Authors. Advanced Materials Interfaces published by Wiley-VCH GmbH. This is an open access article under the terms of the Creative Commons Attribution License, which permits use, distribution and reproduction in any medium, provided the original work is properly cited.

DOI: 10.1002/admi.202300668

B. Heidrich, M. Winter
MEET Battery Research Center, Institute of Physical Chemistry
University of Münster
48149 Münster, Germany
C. Gammer
Erich Schmid Institute of Materials Science
Austrian Academy of Sciences
Leoben 8700, Austria
M. Winter
Helmholtz Institute Münster, IEK-12
Forschungszentrum Jülich GmbH

48149 Münster, Germany





www.advmatinterfaces.de

charge cut-off voltages.^[6-9] Despite the high theoretical capacity of Ni-rich NMC electrode, the high amount of Ni ions make the NMC structure unstable at high charge cut-off voltages. NMC-111 electrode has a higher chemical and structural stability during electrochemical cycling compared to the Ni-rich NMC electrode.[10-13] The deterioration factors causing the NMC capacity fading are: microcrack formation within secondary particles, cation mixing, oxygen evolution, dissolution of transition metals (TM) into the liquid electrolyte, Jahn-Teller distortion, HF etching induced by the electrolyte decomposition, cathode - electrolyte interface (CEI) formation, and surface reconstruction. [14-26] It has been shown that the surface modifications by a coating layer consisting of a metal oxide prohibit the aforementioned deterioration factors and improve the capacity retention at high charge cut-off voltages. [27-29] The effect of different metal oxides such as Al₂O₃, TiO₂, ZnO, and MgO on the capacity retention and rate capability of NMC electrodes has been studied. [30-40] Despite the high corrosion resistance of ZnO, its electronic conductivity is low. However, it has been shown that Al:ZnO has high electronic conductivity and a good lattice compatibility with LiCoO2 electrode compared to other metal oxides.[41,42] Since the side reactions that occur at the electrode/electrolyte interface influence the kinetics of Li-ion diffusion, electron exchange and cycle life, it is necessary to study and control the reactions occurring at the electrode/electrolyte interface in order to improve the electrochemical performance of LIBs.[43,44] It has been shown that during the post-annealing process of the coatings, the metal ions (e.g., Al3+, Mg2+) diffuse into the surface and stabilize the electrode/electrolyte interface by forming a solid solution between the electrode surface and the coating layer. [45,46] Although the electrochemical studies have shown that the surface coatings improve the capacity retention of cathode materials, understanding the underlying suppression mechanism induced by the coating layer at the electrode/electrolyte interface is necessary. Transmission electron microscopy (TEM) is an ideal tool for probing the interfacial reactions as the thickness of the electrode/electrolyte interfacial region is in the range of a few nano-meters. [47,48] Electron energy-loss spectroscopy (EELS) is capable of detecting Li⁺ ions and also studying the electronic structure change of oxygen and TM ions that occur at the electrode/electrolyte interface during charging/discharging.[49] Using nano-beam electron diffraction (NBD) it is possible to study the local structural changes at the nano-scale.^[50] The structural and chemical changes in the bulk and at the surface of uncoated NMC electrodes cycled in different voltage ranges were studied using TEM. The TEM studies of the structure and chemistry of uncoated NMC-111 electrode before and after electrochemical cycling show that a phase transformation from a layered (R-3m space group) to a spinel (Fd-3m space group) and then to a rock-salt (Fm-3m space group) structure and the reduction of the oxidation state of the TM ions occurred at the electrode surface that was in direct contact with the electrolyte, causing capacity fading and impedance growth. [16,34,51,52] Moreover, the phase transformation and the reduction of the oxidation state of TM ions at the electrode surface has already been reported in TEM studies of LiNi_{0.6}Mn_{0.2}Co_{0.2}O₂ (NMC-622), LiNi_{0.5}Mn_{0.3}Co_{0.2}O₂ (NMC-532), and LiNi_{0.8}Mn_{0.1}Co_{0.1}O₂ (NMC-811) electrodes. [53–56] A TEM study of a NMC electrode has shown that the primary particles located in the core of secondary particles do not experience a significant phase transformation at the surface compared to the primary particles that are in contact with the electrolyte.^[57] However, a systematic TEM study focusing on the effect of an Al:ZnO coating layer on the structural and chemical stabilities of NMC-111 electrodes cycled at high charge cut-off voltages has not been reported yet.

In this work, an Al:ZnO coating layer was deposited onto NMC-111 commercial powder electrode using a microwaveassisted sol-gel synthesis method. The atomic and electronic structures of uncoated and Al:ZnO - coated NMC-111 electrodes before and after electrochemical cycling in the high voltage range of 3.0 - 4.5 V were studied using high resolution - TEM (HR-TEM) and scanning TEM (STEM) imaging combined with NBD and EELS. HR-TEM image and NBD pattern of the uncoated NMC -111 electrodes after 50 cycles show that a significant structural change occurred at the electrode surface and EELS analyses indicate a change of the electronic structure at the electrode surface. Whereas, the Al:ZnO coating layer suppressed the aforementioned crystal - and electronic structure changes at the electrode surface/coating layer interface, improving the capacity retention and rate capability. A functional mechanism of the surface coating has been proposed and its effect on the structural and chemical changes of the electrode bulk and surface has been investigated.

2. Results and Discussion

2.1. Structural and Chemical Analysis of the Pristine NMC-111 Electrode

The XRD pattern of pristine uncoated and Al:ZnO – coated NMC-111 electrodes are shown in Figure 1b. XRD shows that the NMC-111 electrode has a trigonal layered (R-3m space group) structure in which TM and Li+ ions occupied the octahedral sites between the oxygen layers as shown in the atomic model in [120] zone axis which is consistent with the previous studies (Figure 1a). $^{[13,16]}$ The XRD pattern of the pristine Al:ZnO – coated NMC-111 electrode shows that no peak related to the hexagonal structure (P63mc space group) of the ZnO coating layer can be seen. However, a small peak related to ZnO can be seen in the magnified XRD pattern from Figure 1b, indicating that the amount of Al:ZnO coating material is very small (Figure S7a, Supporting Information). $^{[58]}$ Moreover, the I_{003}/I_{014} peak intensity ratio in the case of the Al:ZnO - coated NMC-111 electrode is higher than that of the uncoated NMC-111 electrode, implying that the coating layer reduces the Li+/Ni2+ cation mixing (Figure 1b). [59,60] The morphology of the pristine uncoated NMC-111 electrode is shown in Figure 1d, demonstrating a large secondary particle which is composed of numerous primary particles. Moreover, the presence of Al:ZnO coating nanoparticles covering the surface of an NMC-111 secondary particle is shown in Figure 1c.

The HAADF- and BF-STEM images of the pristine uncoated NMC -111 electrode show the primary particles with the particle size in the range of 500 nm–1 μ m (Figures S1a,S2, Supporting Information). HR-TEM, HR-HAADF, and HR-DF-STEM images of the pristine uncoated NMC-111 electrode are shown in Figure S1b–e (Supporting Information). HR-TEM and HR-HAADF-STEM images show a trigonal layered structure (R-3m space group) at both (001) – (Figure S1b, Supporting

entrum Jülich GmbH Research Center, Wiley Online Library on [27/02/2024]. See the Terms and Conditions (https://onlinelibrary.wiley.

onditions) on Wiley Online Library for rules of use; OA articles are governed by the applicable Creative Commons

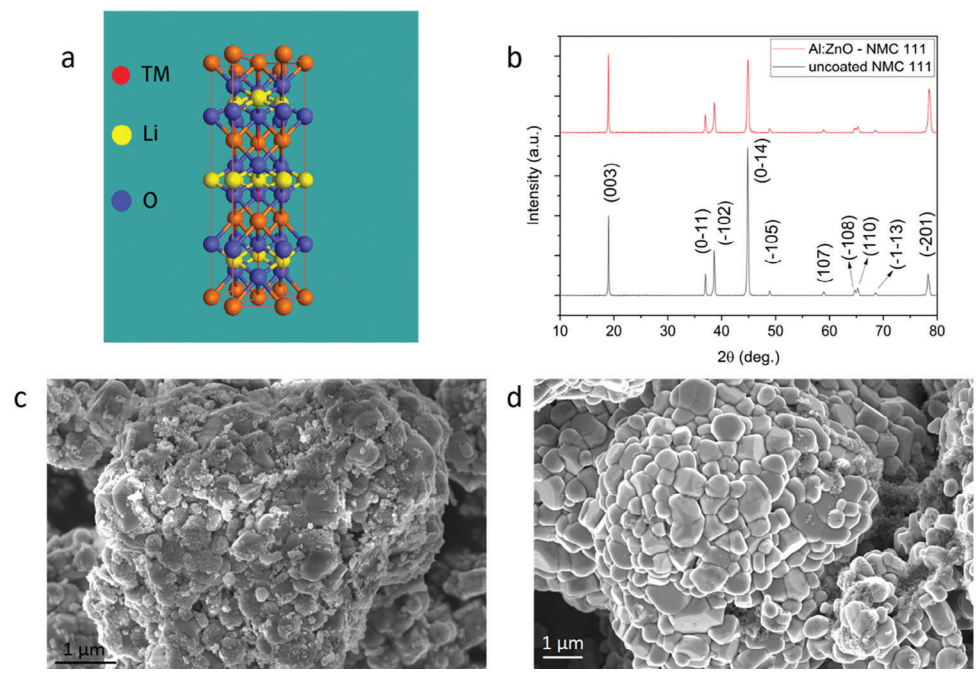


Figure 1. a) Atomic model of LiTMO₂ (TM: Ni, Mn, and Co) showing the atomic arrangement in [120] zone axis drawn by the JEMS software, ^[61] b) XRD pattern of the pristine uncoated and Al:ZnO – coated NMC-111 electrodes confirming the trigonal layered structure (R-3m space group), and SEM images of the pristine c) Al:ZnO coated and d) uncoated NMC-111 electrodes.

Information) and non - (001) surfaces (Figure S1c,d, Supporting Information). A HR-DF-STEM image shows that the crystal structure in the bulk is trigonal layered (Figure S1e, Supporting Information). The NBD pattern acquired in [100] zone axis from the bulk also indicates a trigonal layered structure of the pristine uncoated NMC-111 electrode (Figure S1f, Supporting Information). In the case of the pristine Al:ZnO - coated NMC-111 electrode, TEM, HAADF-, and BF-STEM images show that the Al:ZnO coating layer covered the secondary particle surface with a high coverage fraction (Figure 2a; Figure S6, Supporting Information). BF-STEM images of the pristine Al:ZnO - coated NMC-111 secondary particle show the coating layer and primary particles with different sizes (Figure S9, Supporting Information). The electron diffraction pattern acquired from the pristine Al:ZnO - coated NMC-111 electrode shows a ploycrystalline structure of the secondary particle as shown in Figure S7b (Supporting Information). The HR-TEM images of the pristine Al:ZnO – coated NMC-111 electrode show that the trigonal layered structure was preserved at the (001) and non – (001) surfaces after the coating process and the post-annealing and no significant structural change occurred at the electrode surface/coating layer interface (Figure 2b,c). The trigonal layered structure in the bulk and at grain boundaries is shown in Figure 2d. The NBD patterns, acquired from the electrode bulk and the coating layer, show a trigonal layered structure (R-3m space group) in [100] zone axis and a hexagonal structure (P63mc space group) in [708] zone axis, respectively (Figure 2e,f).

The EDX elemental map and line-profile of a pristine uncoated NMC-111 electrode show a homogeneous distribution of Ni, Mn, and Co throughout the particle and a slightly higher concentration of O at the surface (Figure S3, Supporting Information). In

the case of the pristine Al:ZnO – coated NMC-111 electrode, the EDX elemental map and line-profile also confirm the homogeneous distribution of Ni, Mn, and Co throughout the particle and also the presence of the Al:ZnO coating layer with a high coverage on the particle surface is shown (Figure S8, Supporting Information). The EDX elemental map and line-profile, acquired from the bulk of the secondary particle, also show that the Al:ZnO coating layer is present along the cavities between the primary particles (Figure S10, Supporting Information).

EELS was performed to study the electronic structure at the surface and in the bulk of pristine NMC - 111 electrodes. Coreloss EELS spectra, acquired form the surface and bulk of the pristine uncoated NMC-111 electrode, shows that no detectable chemical shift of the Co-L₃, Mn-L₃, and Ni-L₃ edges can be seen, revealing that the oxidation state of the Ni, Mn, and Co ions is constant at the surface and in the bulk (Figure S4a,c-e, Supporting Information). Moreover, the O-K edge pre-peak, which is related to the O 2p states hybridized with the transition metal 3d states reflecting the oxidation state and coordination change of TM ions, shows no intensity change and chemical shift (Figure S4a,b, Supporting Information). [62,49] From the coreloss EELS spectra of the pristine uncoated NMC -111 electrode, the oxidation state of three TM ions are determined which are Mn⁴⁺, Co³⁺, and Ni²⁺. [16,63] In the case of the pristine Al:ZnO – coated NMC -111 electrode, core-loss EELS spectra acquired form the surface/coating layer interface and from the bulk show that the Co-L₃ and Mn-L₃ edges were chemically shifted to lower energies, implying that the oxidation state of the Co and Mn ions was reduced at the surface/coating layer interface compared to the bulk (Figure 3a,f,g). Whereas no chemical shift of the Ni-L₃ edge occurred at the surface/coating layer interface

and-conditions) on Wiley Online Library for rules of use; OA articles are governed by the applicable Creative Commons

www.advancedsciencenews.com



www.advmatinterfaces.de

a NMC-111 Al:ZnO

Pt Al:ZnO

R[100]

(120)

(123)

5 1/nm

C <001>
R[708]

(223)

(120)

(103)

5 1/nm

Figure 2. TEM imaging and NBD pattern of a pristine Al:ZnO – coated NMC-111 electrode: a) TEM image, b) HR-TEM image, and c) magnified HR-TEM image, acquired from the square shown in (b), show a trigonal layered structure (R-3m space group) at the surface and the surface/coating layer interface, d) HR-TEM image of the electrode bulk including grain boundaries and a triple junction shows a trigonal layered structure, NBD pattern acquired from e) the electrode bulk in [100] zone axis, and f) the coating layer in [708] zone axis.

(Figure 3a,e). Moreover, the O-K edge pre-peak, acquired from the surface/coating layer interface and from the bulk, show that the O-K edge pre-peak disappeared at the surface/coating layer interface compared to the bulk, confirming that the oxidation state of Co and Mn ions reduced at the surface/coating layer interface (Figure 3a,c). The O-K edge EELS spectra acquired from the Al:ZnO coating layer shows that no pre-peak can be seen, implying a significant change of the coordination environment of oxygen ions (Figure 3a,b). The L_3/L_2 intensity ratios of the Co-L_{2,3}, Mn-L_{2,3}, and Ni-L_{2,3} edges, as a function of distance from the surface/coating layer interface also shows the reduction of the oxidation states of Mn and Co ions and no significant change of the oxidation state of Ni ions at the surface/coating layer interface. Moreover, the L_3/L_2 intensity ratio analysis also shows that a surface reduction layer with a thickness ≈7.5 nm was formed at the surface/coating layer interface (Figure 3d).

EELS elemental mapping of the pristine uncoated NMC-111 electrode shows a homogeneous distribution of Ni, Mn, and Co and a slightly higher concentration of O at the surface (Figure S5, Supporting Information), which is consistent with the EDX mapping and line-profile as shown in Figure S3 (Supporting Information). EELS elemental mapping of the pristine Al:ZnO - coated NMC-111 electrode shows that the concentration of Mn ions at the surface/coating layer interface is high, and the Co and Ni ions are present in the coating layer (Figure S11, Supporting Information). Moreover, the core-loss EELS spectra acquired from the Al:ZnO coating layer also confirm the presence of Co and Ni ions in the coating layer (Figure S12a,b, Supporting Information). The core-loss EELS spectra acquired from the surface and surface/coating layer interface show that the Al-L₁, Al-L_{2,3}, Zn-M₁, and Zn-M_{2,3} peaks are present at the surface/coating layer interface, revealing that the Zn and Al ions diffused into the electrode surface during the microwave-based annealing at 180°C (Figure S12a,b, Supporting Information).^[45,64] The Li-K edge EELS spectra, acquired from the surface near to the coating layer and the bulk, shows a homogeneous distribution of Li⁺ ions (Figure S12a,c, Supporting Information). EELS data, HR-TEM images, and NBD pattern of the pristine Al:ZnO – coated NMC-111 electrode show that, due to the presence of the coating layer and post-annealing, a solid solution was formed at the surface/coating layer interface.^[64]

2.2. Electrochemical Performance of the NMC-111 Electrode

The cyclic stability and rate capability of the uncoated and Al:ZnO - coated NMC-111 electrodes at different charge cut-off voltages are shown in Figure 4. In case of the uncoated NMC-111 electrode, cycled at 3.0-4.5 V, the 1st discharge capacity is 159 mAhg⁻¹ and subsequently capacity fading occurred. In case of the Al:ZnO - coated NMC-111 electrode, cycled at 3.0-4.5 V, the 1st discharge capacity increased to 186 mAhg⁻¹ and the capacity retention has been improved (Figure 4a). The rate capability of uncoated NMC-111 electrode cycled at 3.0-4.2 V shows capacity loss and low rate capability. Whereas in the case of Al:ZnO – coated NMC-111 electrode cycled at 3.0–4.5 V, a significant improvement of the rate capability can be seen, revealing that the coating layer improved the electronic conductivity and the Li⁺ diffusion kinetics and the doped Al ions improved the electronic conductivity of ZnO as reported in a previous study (Figure 4b). [65] It has been shown that the electronic conductivity of Al:ZnO is high as its resistivity value is in the range of 10^{-2} and $10^{-3}~\Omega$ cm.^[66] Moreover, it has been reported that the Li⁺ ion diffusion coefficient in ZnO is in the range of 10^{-14} – 10^{-12} cm² s⁻¹,

21967350, 2024, 2, Downloaded from https

rch Center, Wiley Online Library on [27/02/2024]. See the Terms

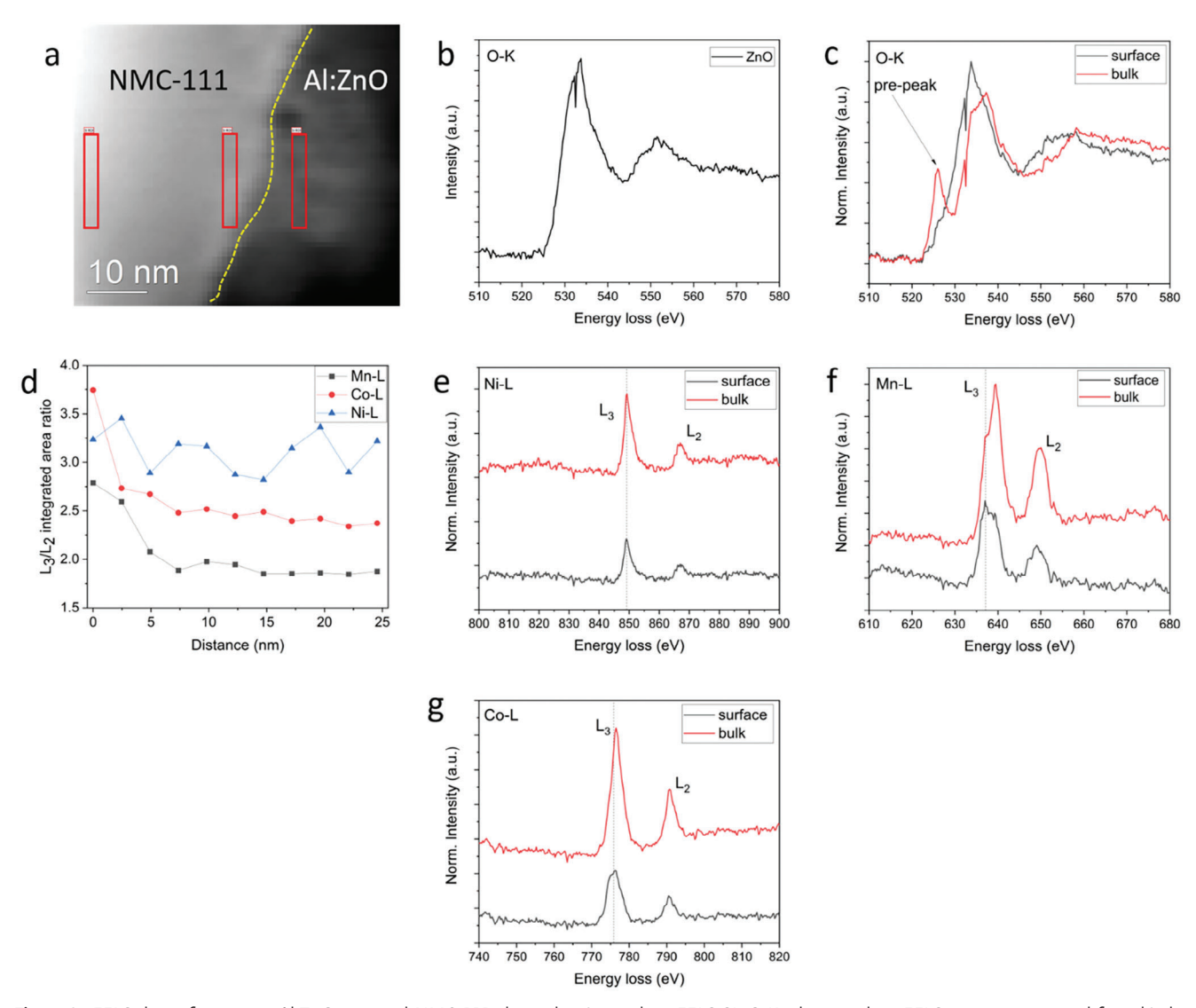


Figure 3. EELS data of a pristine Al:ZnO – coated NMC-111 electrode: a) core loss EELS-SI, O-K edge core-loss EELS spectra integrated from b) the coating layer, c) the surface/coating layer interface and bulk (rectangles as shown in (a)), d) L_3/L_2 intensity ratio as a function of distance from the surface/coating layer interface, and e–g) Mn- $L_{2,3}$, Co- $L_{2,3}$, and Ni- $L_{2,3}$ edge core-loss EELS spectra, integrated from the rectangles shown in (a), showing the reduction of the oxidation states of Mn and Co ions at the surface/coating layer interface compared to the bulk.

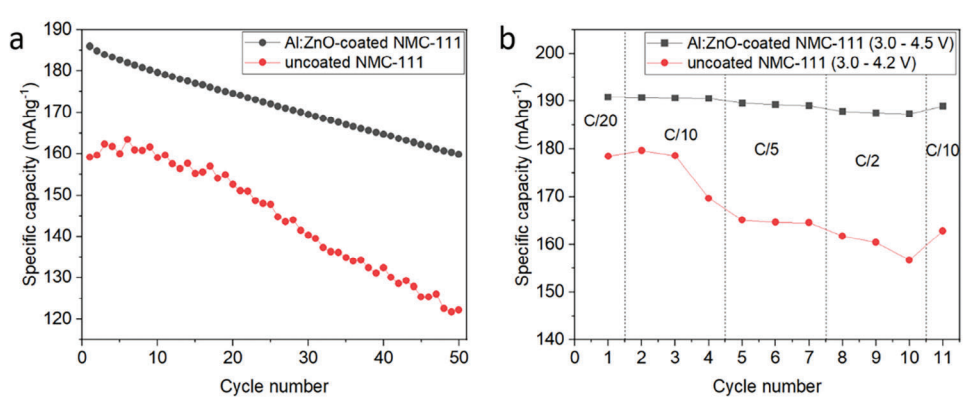


Figure 4. a) Cyclic stability measurement of the uncoated and Al:ZnO – coated NMC-111 electrodes in the voltage range of 3.0–4.5 V at C/2, b) rate capability of the uncoated and Al:ZnO – coated NMC-111 electrodes in the voltage ranges of 3.0–4.2 V and 3.0–4.5 V, respectively.



www.advmatinterfaces.de

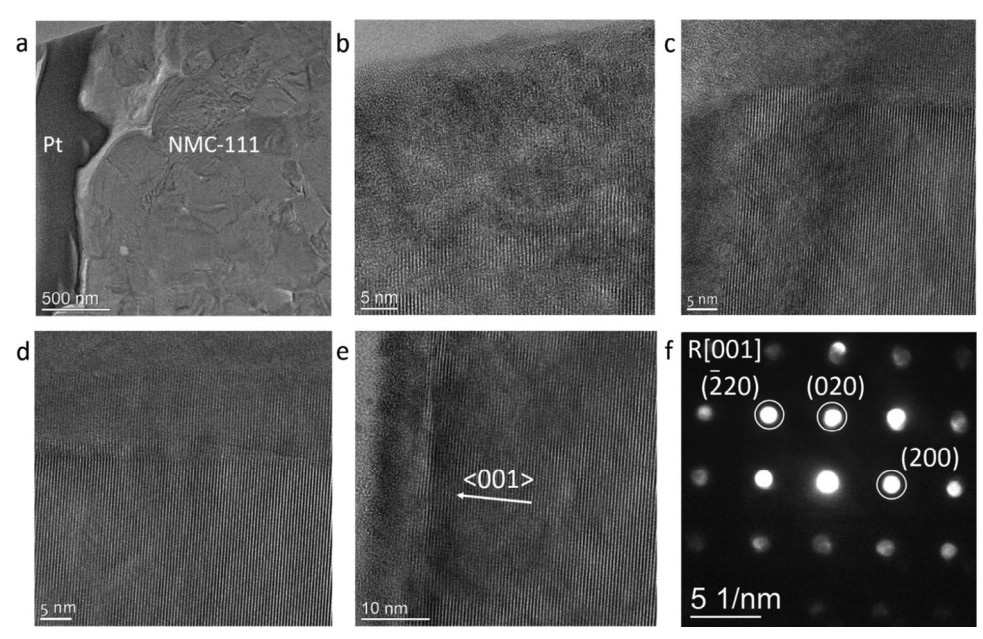


Figure 5. TEM imaging and NBD pattern of an uncoated NMC-111 electrode after 50 cycles in the voltage range of 3.0–4.5 V: a) TEM and b–e) HR-TEM images acquired from the electrode surface and the bulk, showing that pitting corrosion, lattice distortions and a phase transformation from a trigonal layered to a rock-salt phase occurred at the surface, and f) NBD pattern in [001] zone axis acquired from the electrode surface.

implying that the diffusion kinetics of Li⁺ ion has been increased by the ZnO coating layer.^[67] An electrochemical impedance spectroscopy (EIS) study has shown that the Al:ZnO coating layer decreased the charge transfer resistance, meaning that the electronic conductivity increased, which is consistent with the improvement in the rate capability.^[68,69]

2.3. Structural and Chemical Analysis of the Uncoated NMC-111 Electrodes after Electrochemical Cycling

TEM images and NBD pattern were acquired to study the structural changes of the bulk and the surface of uncoated NMC-111 electrodes after electrochemical cycling in the voltage range of 3.0-4.5 V. TEM and HR-TEM images of the uncoated NMC-111 electrodes after 50 cycles are shown in Figure 5a-e. HR-TEM images, taken from different primary particle surface and bulk regions, show that due to a direct electrolyte exposure and unwanted side reactions at the electrode/electrolyte interface, pitting corrosion, lattice distortions and a phase transformation from a trigonal layered (R-3m space group) to a rock-salt (Fm-3m space group) phase occurred and a surface reconstruction layer formed at the electrode surface. Moreover, the trigonal layered structure was preserved in the bulk after 50 cycles (Figure 5a-e). It has been shown that the phase transformation and formation of the surface reconstruction layer occurred in the case of the NMC electrode, which was exposed to the electrolyte before electrochemical cycling, leading to a reduction of the coulombic efficiency in the 1st cycle. [20] The thickness of the surface reconstruction layer of the NMC electrode increased during cycling at high charge cut-off voltages. [20,51] The formation of the rock-salt phase results in a reduction of the diffusion kinetics of the Li+ ions due to the reduction of Li^+ active sites occupied by TM ions

and due to an increase of the diffusion barriers for Li+ intercalation/deintercalation. This leads to capacity fading as shown in Figure 4a.[16,20,51] The NBD pattern in [001] zone axis, acquired from different regions of the electrode surface, shows that the thickness of the surface reconstruction layer in some primary particles is significantly higher than in other particles, which has been reported before (Figure 5f). [16] The thickness variation of the surface reconstruction layer is due to the fact that the extent of phase transformation on certain surface facets of the NMC crystal structure is more significant than on other surface facets.^[20,51] The surface reconstruction layer was developed at both (001) and non - (001) surfaces of the uncoated NMC-111 electrodes after 50 cycles. However, the thickness of the surface reconstruction layer along the Li⁺ diffusion channels (non - (001) surface) is larger than that at the (001) surface, since the removal of the Li⁺ ions occurred along the Li⁺ diffusion channels during charging, which increased the thickness of the surface reconstruction layer (Figure 5b-e).[20,51] A density functional theory (DFT) study has shown that when \approx 60% of Li⁺ ions are removed from the NMC crystal structure during charging at high cut-off voltage, the layered to rock-salt phase transformation at the electrode surface become favorable. [20] The HAADF – and BF-STEM images of uncoated NMC-111 electrodes after 50 cycles show that the contrast changed in some regions, revealing that a dislocation-like defect formed and strain developed due to the volume change during lithiation and de-lithiation (Figure S14, Supporting Information). The plane – view and cross – sectional SEM images show that the morphology of uncoated NMC-111 electrodes did not change significantly after 50 cycles and small particles related to the CEI layer formed at the secondary particle surface (Figure S13a-c, Supporting Information).

An EEL'S study, performed on the uncoated NMC –111 electrodes during the 1st cycle at different states of charging (SOC),

ons) on Wiley Online Library for rules of use; OA articles are governed by the applicable Creative Commons

www.advmatinterfaces.de

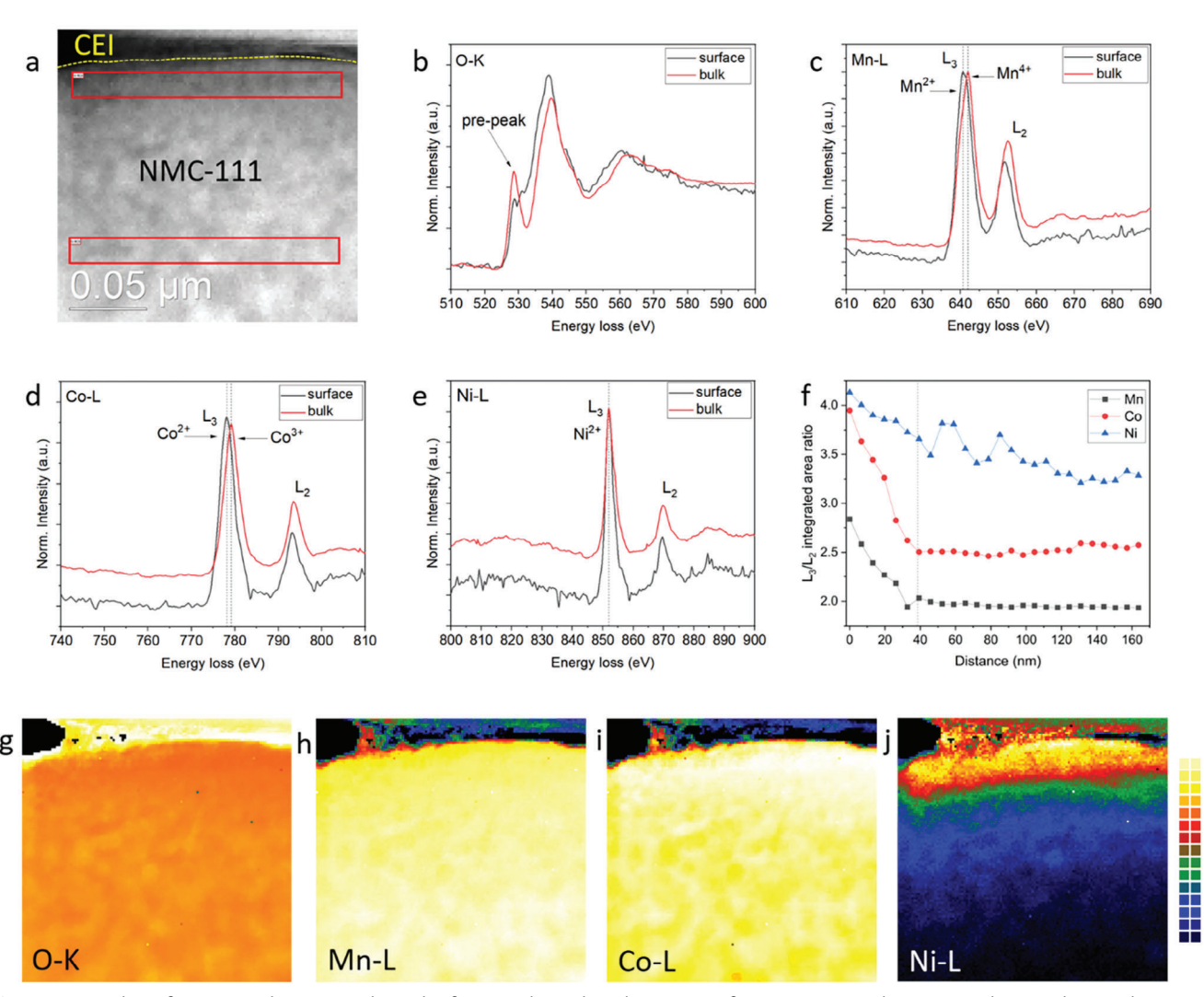


Figure 6. EELS data of an uncoated NMC-111 electrode after 50 cycles in the voltage range of 3.0–4.5 V: a) core-loss EELS-SI, b) O-K edge core-loss EELS spectra integrated from the rectangles shown in (a), c) Mn-L_{2,3}, d) Co-L_{2,3}, and e) Ni-L_{2,3} edge core-loss EELS spectra integrated from the rectangles shown in (a), showing a significant reduction of the oxidation state of the Co and Mn ions at the electrode surface compared to the bulk, whereas no change in the oxidation state of the Ni ions can be seen, f) L₃/L₂ intensity ratio as a function of distance from the surface, g–j) EELS elemental map of oxygen, Mn, Co, and Ni (the temperature color scale from dark blue to light yellow exhibits an increase in relative elemental concentration (at%)).

shows that the Ni-L₃ edge EELS spectra, acquired from the bulk, shifted to higher energies during charging and shifted to lower energies during discharging. No obvious peak shift of the Mn-L₃ and Co-L3 edge EELS spectra were shown during charging and discharging, revealing that Ni²⁺ ≠ Ni⁴⁺ redox reaction occurred in order to compensate the charge transfer during charging and discharging. In contrast, the Mn⁴⁺ and Co³⁺ ions were inactive during charging and discharging.[16] Moreover, it has been shown that the oxidation state of Mn, Co, and Ni ions at the surface of uncoated NMC-111 electrodes reduced, compared to the bulk during the 1st charging (de-lithiation) and a surface reduction layer was formed.[16,70] It has been reported that a thin surface reduction layer was formed at the surface of uncoated NMC electrode which was in contact with the electrolyte before electrochemical cycling. [20] The formation of a surface reduction layer at the electrode surface is due to the kinetic effect of Li⁺ diffusion during charging which primarily occurred at the electrode surface, re-

sulting in a high number of Li⁺ vacancies formed at the electrode surface causing the TM/Li⁺ cation mixing. [70] Moreover, it was revealed that the oxidized Ni⁴⁺ ions, formed at the electrode surface during charging, react with the electrolyte and reduce to soluble Ni²⁺ ions, causing the electrolyte decomposition and also the formation of the surface reduction layer. [16,71]

The EELS data of uncoated NMC-111 electrodes after 50 cycles in the voltage range of 3.0–4.5 V are shown in **Figure 6**. The core-loss EELS spectra, acquired form the surface and the bulk, shows a chemical shift of the Mn-L $_3$ and Co-L $_3$ edges to lower energies confirming that, due to a direct electrolyte exposure, the reduction of the oxidation state of the Mn and Co ions occurred at the electrode surface. The energy position of the Mn-L $_3$ and Co-L $_3$ edges show that the oxidation state of Mn⁴⁺ reduced to Mn²⁺ and the oxidation state of Co³⁺ reduced to Co²⁺ at the electrode surface, whereas the oxidation states of Mn⁴⁺ and Co³⁺ ions in the bulk were the same as that of pristine NMC-111 electrodes,

ADVANCED SCIENCE NEWS

www.advancedsciencenews.com



www.advmatinterfaces.de

revealing the presence of a surface reduction layer at the surface after 50 cycles (Figure 6a,c,d).^[20] The energy position of Ni-L₃ edge EELS spectra, acquired from the surface and bulk, shows that no Ni-L₂ edge chemical shift occurred at the electrode surface, revealing that the oxidation state of the Ni²⁺ ions was constant from the electrode surface to the bulk, since the electrode was in the discharged state after 50 cycles (Figure 6a,e).[16,51] Figure S25 (Supporting Information) shows a series of core-loss EELS spectra acquired from the surface to the bulk of an uncoated NMC-111 electrode after 50 cycles. The series of Co-L_{2,3}, Mn-L23, and Ni-L23 edge EELS spectra also show the chemical shift of the Mn-L3 and Co-L3 edges to lower energies at the surface (Figure S25b-d, Supporting Information). The O-K edge EELS spectra, acquired from the electrode surface and bulk, shows that the O-K edge pre-peak shifted to higher energies and its intensity significantly reduced at the surface of the uncoated NMC-111 electrode, showing that a significant oxygen loss, the reduction of the oxidation state of the Mn and Co ions and oxygen vacancy formation occurred at the electrode surface after 50 cycles at a charge cut-off voltage of 4.5 V (Figure 6a,b). [62] The series of O-K edge EELS spectra, acquired from the surface to the bulk, also shows a significant reduction of the intensity of the O-K edge pre-peak and the disappearance of the O-K edge pre-peak at the outermost electrode surface due to the oxidation state reduction of the Co and Mn ions and the oxygen vacancy formation at the surface (Figure S25a, Supporting Information). [62] The formation of a large number of oxygen vacancies weaken the electrostatic attraction between the TM and the oxygen ions remained in the crystal structure of the NMC electrode. [52] It was reported that the significant reduction of the O-K edge pre-peak intensity at the electrode surface is due to the movement of TM ions into the free Li+ ion sites during charging, causing a significant change in O 2p and TM 3d hybridized states.[16,52] Moreover, it has been shown that during charging at high cut-off voltage, oxygen ions migrate from the bulk to the surface of NMC-111 electrodes at which a portion of these ions are released as active oxygen species.^[72] The irreversible phase transformation from a layered to a disordered rock-salt phase and the formation of a surface reconstruction layer is due to the movement of TM ions into the Li+ ion free sites during charging in the octahedral sites within the identical oxygen framework.[16,52] It has been shown that the energy barrier for the migration of Co and Mn ions into the Li⁺ ion free sites is higher than that of Ni ions.^[73,74] Moreover, due to the similar ionic radius of Ni²⁺ and Li⁺ ions and the low energy barrier for the migration of Ni ions into the Li⁺ ion free sites, the surface reconstruction layer formation occurred mostly due to the Ni/Li+ cation mixing.[75,76]

The L_3/L_2 intensity ratio of the Mn- $L_{2,3}$, Co- $L_{2,3}$, and Ni- $L_{2,3}$ edge EELS spectra, as a function of distance from the electrode surface, also confirm the reduction of the oxidation state of the Mn and Co ions and the formation of a surface reduction layer at the surface of uncoated NMC -111 electrode after 50 cycles (Figure 6f). The thickness of surface reduction layer at the surface is ≈ 40 nm, as shown by a dashed line in Figure 6f, revealing that the thickness of surface reduction layer, formed during the 1st charging, increased during the following cycles. [16,51]

The low-loss EELS spectra, acquired from the surface to the bulk of an uncoated NMC-111 electrode after 50 cycles, shows that the Li-K edge intensity disappeared at the electrode surface,

revealing that Li⁺ ion loss occurred which is related to the Ni/Li⁺ cation mixing at the electrode surface (Figure S15, Supporting Information).[20,51] Moreover, the EELS elemental map and the corresponding O, Mn/O, Co/O, and Ni/O ratio line-profiles, as functions of the distance from the electrode surface, also confirm that oxygen loss occurred at the electrode surface, which is consistent with the EDX elemental map and line-profile as shown in Figure 6g and Figures S18,S20d,i (Supporting Information).[77] Moreover, the EELS elemental map shows that the concentration of Ni and Co ions is high at the electrode surface compared to the bulk, revealing that the TM ions segregated at the electrode surface, which can be due to a significant TM/Li+ cation mixing (Figure 6h-j).[51,78] The EDX elemental map and line-profile also show that a thick CEI layer was formed on the surface of the uncoated NMC-111 electrode after 50 cycles, meaning that due to a severe interaction between the electrode and electrolyte, the electrolyte decomposition products (e.g., Li₂CO₃ and LiF) were formed (Figure S20b,c,i, Supporting Information). [79,80] It has been shown that LiPF₆ salt decomposes and HF forms according to the following reactions:[81]

$$LiPF_6 \rightarrow LiF(s) + PF_5$$
 (1)

$$H_2O + PF_5 \rightarrow POF_3 + 2HF$$
 (2)

It has been reported that the HF dissociation reactions etched the electrode surface and formed LiF species and H₂O, accelerating the electrode degradation by forming additional HF (reaction [2]).^[81] The LiF species precipitated on the electrode surface and blocked the Li⁺ ion diffusion channels, contributing to the impedance increase at the electrode/electrolyte interface and to capacity fading.^[81] Moreover, the EDX elemental map and lineprofile of the uncoated NMC-111 electrode after 50 cycles show that the TM ions were present in the CEI layer, which is consistent with the EELS results as shown in Figure 6h–j. The presence of TM ions in the CEI layer indicates that TM ion dissolution into the electrolyte occurred, which also leads to capacity fading (Figure S20e–g,i, Supporting Information).^[25]

2.4. Structural and Chemical Analysis of Al:ZnO – Coated NMC-111 Electrodes after Electrochemical Cycling

HR-TEM image and NBD pattern were acquired to study the structural changes at the surface/coating layer interface and in the bulk of Al:ZnO - coated NMC-111 electrodes after electrochemical cycling in the voltage range of 3.0-4.5 V. HR-TEM images of Al:ZnO - coated NMC-111 electrodes after 50 cycles are shown in Figure 7. HR-TEM images show that due to the presence of a coating layer, no rock-salt structure can be seen, meaning that no irreversible phase transformation from a trigonal layered to a rock – salt structure occurred along the Li⁺ diffusion channels (non - (001) surface). This means that the surface reconstruction layer did not form and the TM and Li⁺ ions still occupied the octahedral sites at the non - (001) surface near to the coating layer. Moreover, HR-TEM images show that no significantly corroded structure was observed, implying that no significant pitting corrosion occurred at the non - (001) surface and the coating layer protected the surface and suppressed the interfacial side reactions at the electrode/electrolyte interface (e.g.,

ditions) on Wiley Online Library for rules of use; OA articles are governed by the applicable Creative Commons

www.advancedsciencenews.com



www.advmatinterfaces.de

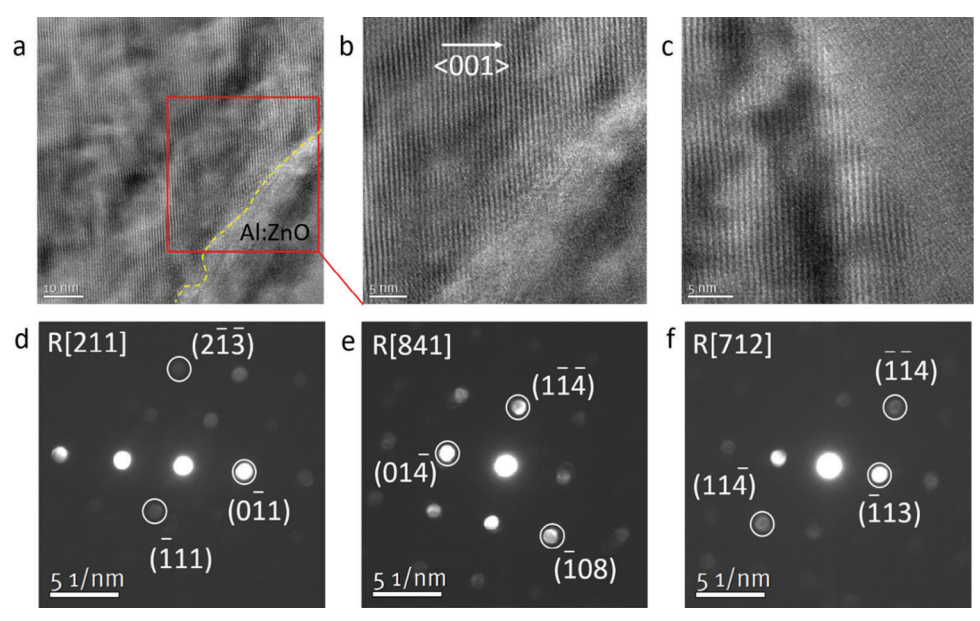


Figure 7. HR-TEM and NBD pattern of an Al:ZnO – coated NMC-111 electrode after 50 cycles in the voltage range of 3.0–4.5 V: a) HR-TEM image and b) magnified HR-TEM image from the square shown in (a) acquired from the electrode surface, c) HR-TEM image from the electrode surface, showing that no irreversible phase transformation from a trigonal layered to a rock – salt structure occurred at the surface, NBD pattern acquired from d) the bulk in [211] zone axis, e) surface in [841] zone axis, and f) coating layer in [712] zone axis.

HF attack) (Figure 7a,b). HR-TEM image acquired from the (001) surface also shows that the layered structure was preserved after 50 cycles (Figure 7c). The NBD pattern acquired from the electrode surface and the bulk also shows the trigonal layered structure in [841] and [211] zone axes, respectively, confirming that the layered structure of the electrode surface was preserved after 50 cycles at the charge cut-off voltage of 4.5 V (Figure 7d,e). Moreover, the NBD pattern acquired from the coating layer shows that the hexagonal structure (P63mc space group) in [712] zone axis was preserved after electrochemical cycling (Figure 2f and Figure 7f). The HAADF- and BF-STEM images confirm that the Al:ZnO coating layer is still present, and no contrast change induced by strain during lithiation and de-lithiation can be seen after 50 cycles (Figure S16, Supporting Information). The plane – view and cross - sectional SEM images of Al:ZnO - coated NMC-111 electrodes after 50 cycles show that nano particles related to the CEI layer formed on the coating layer (Figure S13d-f, Supporting Information).

EELS was performed to study the electronic structure in the bulk and at the surface/coating layer interface of Al:ZnO- coated NMC-111 electrodes after 50 cycles in the voltage range of 3.0–4.5 V. The EELS data of Al:ZnO – coated NMC-111 electrodes after 50 cycles are shown in Figure 8. Core-loss EELS spectra, acquired from the surface near to the coating layer and the bulk, shows that no significant chemical shift of the Co-L₃, Mn-L₃, and Ni-L₃ edges to lower energies occurred, implying that the oxidation state of Co, Mn, and Ni ions did not reduce at the electrode surface. This means that the coating layer suppressed the formation of a surface reduction layer and no significant TM (Ni²⁺)/Li⁺ cation mixing occurred at the electrode surface near to the coating layer. Moreover, the features and energy positions of the Mn-L₃, Co-L₃, and Ni-L₃ edges acquired from the surface near to the coating layer are similar to those acquired from the bulk, indi-

cating the presence of Co³⁺, Mn⁴⁺, and Ni²⁺ ions (Figure 8a,g-i). The O-K edge EELS spectra, acquired from the same region, also shows that the reduction of the intensity of the O-K edge pre-peak or the chemical shift did not occur, implying that the coordination change of TM ions, the reduction of the oxidation state of the Co³⁺ and Mn⁴⁺ ions, and the oxygen vacancy formation did not occur at the surface near to the coating layer (Figure 8a,f). The O-K edge features acquired from the surface near to the coating layer are resembling that acquired from the bulk, implying that the coordination change, and oxidation state reduction of the TM ions did not occur (Figure 8a,f). The Low-loss EELS spectra, acquired from the surface (near to the coating layer) to the bulk, shows that the Li-K peak can be seen, implying that no significant Li+ ion loss or change in the concentration of Li+ ion occurred after 50 cycles (Figure S17, Supporting Information). EELS elemental mapping and corresponding O, Mn/O, Co/O, and Ni/O ratio line-profiles have shown that no significant oxygen loss occurred at the surface near to the coating layer, which is consistent with the EDX elemental map and line-profile (Figure 8b; Figures S19,S21f,k, Supporting Information). The EDX elemental mapping and line-profile of an Al:ZnO - coated NMC-111 electrode show that Mn, Ni, and Co were homogenously distributed throughout the primary particles after 50 cycles. This observation is in good accordance with the EELS elemental map and lineprofile of Mn, Co, and Ni, as shown in Figure 8c-e and Figure S19 (Supporting Information), revealing that no TM ion segregation at the electrode surface occurred (Figure S21g-k, Supporting Information). The presence of O, Ni, Co, and Mn ions in the coating layer indicate that the solid solution, formed during microwavebased heating at 180 °C, is stable during electrochemical cycling at the charge cut-off voltage of 4.5 V (Figure 8b-e; Figure S11, Supporting Information). Moreover, the EDX elemental map and line-profile show that no thick CEI layer was formed. Electrolyte

21967350, 2024, 2, Downloaded from https://onlinelibrary.wiley.com/doi/10.1002/admi.202300668 by Forschun

fülich GmbH Research Center, Wiley Online Library on [27/02/2024]. See the Terms

ditions) on Wiley Online Library for rules of use; OA articles are governed by the applicable Creative Commons

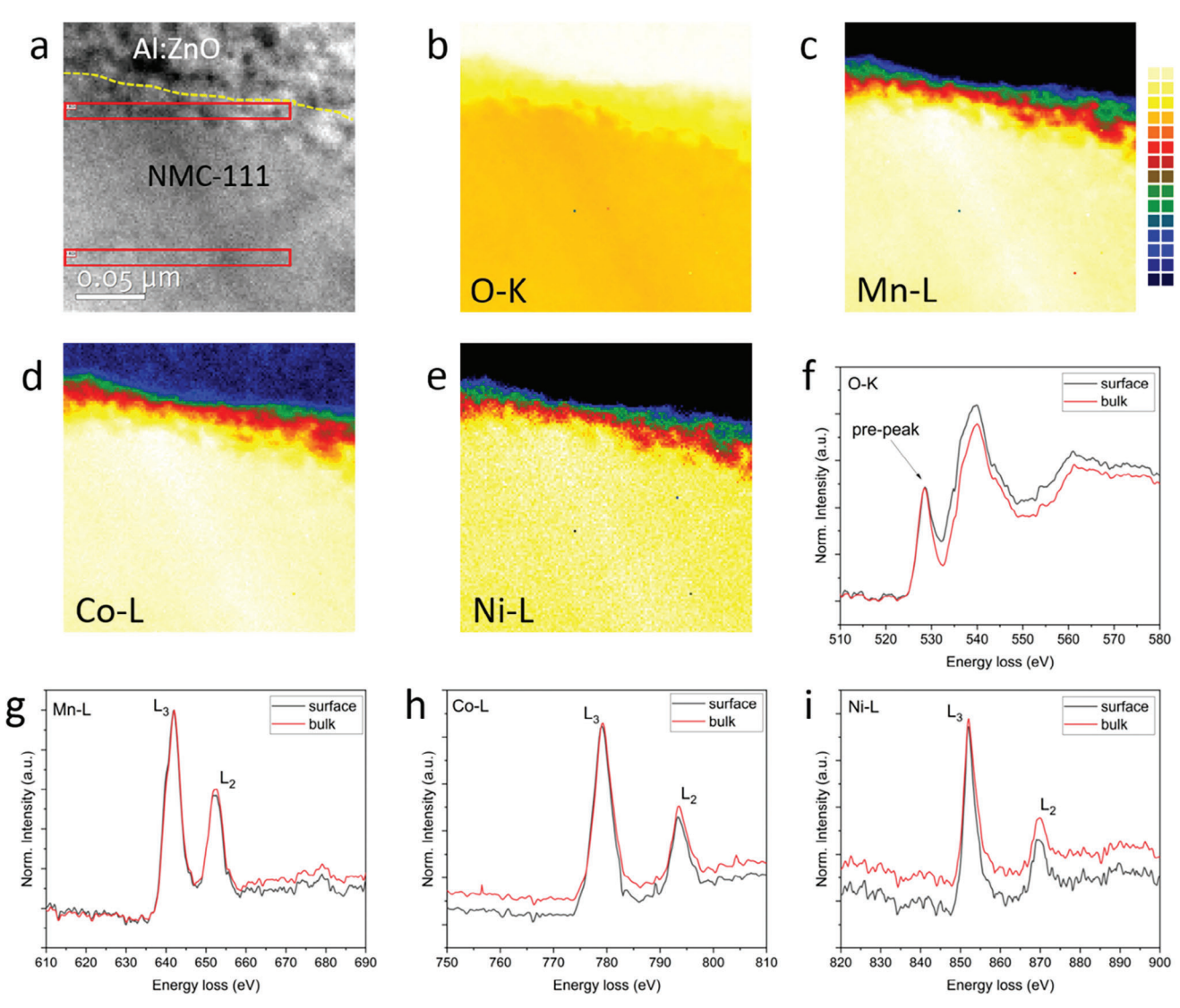


Figure 8. EELS data of an Al:ZnO – coated NMC-111 electrode after 50 cycles in the voltage range of 3.0–4.5 V: a) core-loss EELS-SI, b—e) EELS elemental map of oxygen, Mn, Co, and Ni, f) O-K edge, g) Mn-L_{2,3}, h) Co-L_{2,3}, and i) Ni-L_{2,3} edge core-loss EELS spectra integrated from the rectangles shown in (a), indicating that no significant chemical shift of the Co-L₃, Mn-L₃, and Ni-L₃ edges to lower energies occurred at the surface near to the coating layer (the temperature color scale from dark blue to light yellow exhibits an increase in relative elemental concentration (at%)).

decomposition products (e.g., Li₂CO₃ and LiF) were detected on the coating layer. This implies that the coating layer protected the electrode surface from direct electrolyte exposure (Figure S21b–e,k, Supporting Information). Moreover, no TM ion was detected in the CEI layer, revealing that the TM ion dissolution into the electrolyte was suppressed by the coating layer during cycling in the high voltage range (Figure S21g–k, Supporting Information).

The uncoated and Al:ZnO – coated NMC-111 electrodes before and after 50 cycles in the voltage range of 3.0–4.5 V were studied by XPS to understand the chemical changes that occurred at the electrode surface during electrochemical cycling. XPS survey spectra of the pristine uncoated NMC-111 electrode, the uncoated and Al:ZnO coated NMC-111 electrodes after 50 cycles are shown in Figure S22 (Supporting Information) and the Zn 2p and Zn 3p peaks related to Zn are visible. In the case of the pristine uncoated NMC-111 electrode, the F 1s core spectra show a single

peak at 687 eV related to the C-F bonds of the PVDF binder (Figure S23b, Supporting Information). [82] Moreover, in the case of the pristine uncoated NMC-111 electrode, the C 1s core spectra show three peaks at 284.5 eV related to the C-C and C=C bonds of the carbon black, 286 eV related to the C-H₂ group of the PVDF binder shifted to higher BE due to the close proximity of the C-F₂ groups, and 290.9 eV related to the CO₃²-or C-F₂ groups of the PVDF binder (Figure S23c, Supporting Information).^[82] Additional carbon-containing surface component peaks, such as C-O or C=O, are not similarly well-expressed in the peak structure. In the case of the pristine uncoated NMC-111 electrode, the O 1s core spectra show two peaks at 529.4 eV related to metal oxide (M-O) and 531.8 eV related to metal carbonate, i.e., Li₂CO₃ formed due to the reaction of the NMC electrode with atmospheric CO₂ (Figure S23a, Supporting Information).^[80] In the case of the uncoated NMC -111 electrode after 50 cycles, the F



www.advmatinterfaces.de

1s core spectra show a peak at 685 eV related to metal fluoride, i.e., LiF and a peak at 687.5 eV related to Li_vPF_vO_z, Li_vPF_v, or fluorinated carbon species, such as PVDF, which are not wellseparated (Figure S23b, Supporting Information).[80,83,84] The C 1s core spectra show a peak at 291 eV related to Li₂CO₃ and two peaks at 284.9 eV related to adventitious carbon (C-C) and 286 eV related to the C-O groups due to the oxidative solvent decomposition, confirming the formation of a CEI layer and the electrolyte decomposition products (e.g., LiF, Li₂CO₃) on the surface of the uncoated NMC-111 electrode after 50 cycles (Figure S23b,c, Supporting Information).[85] In the case of Al:ZnO - coated NMC-111 electrode after 50 cycles, the F 1s core spectra show a peak at 685 eV related to LiF and a peak at 687 eV, i.e., at the same position as in the pristine sample (Figure S23b, Supporting Information). A shift of the peak toward higher binding energy, which was the case for the uncoated sample, cannot be observed. Hence, the contribution of Li_xPF_yO_z, Li_xPF_y, or fluorinated carbon species to the F 1s core spectra of Al:ZnO - coated NMC-111 electrode after 50 cycles is notably lower, implying that the electrode surface was protected from direct electrolyte exposure by the coating layer (Figure S23b,d, Supporting Information). The presence of the Li 1s peak also confirms the formation of LiF in the case of the uncoated and Al:ZnO - coated NMC-111 electrodes after 50 cycles (Figure S22, Supporting Information).[86] The C 1s core spectra show a peak at 291 eV related to Li₂CO₃, confirming the formation of the CEI layer and the electrolyte decomposition products on the coating layer of the NMC-111 electrode after 50 cycles, but C-O species are found to a notably lower extent compared to the uncoated sample (Figure S23c, Supporting Information). An XPS survey spectra of an Al:ZnO - coated NMC-111 electrode after 50 cycles shows that the Zn 2p and Zn 3p peaks related to the ZnO coating layer were detected, revealing that the coating layer was intact after 50 cycles (Figure S22, Supporting Information). The Zn 2p core spectra show Zn 2p_{1/2} and Zn 3p_{3/2} peaks at 1044.7 and 1021.6 eV, respectively (Figure S24, Supporting Information). [87] In the case of the pristine uncoated NMC-111 electrode, the O 1s core spectra show a peak at 529.4 eV related to the NMC-111 electrode, whereas this peak disappeared in the case of Al:ZnO coated NMC-111 electrode after 50 cycles due to the presence of the coating layer and also the formation of a CEI layer on the coating layer (Figure S23a, Supporting Information).[82]

A DFT study has shown that a ZnO coating can suppress the HF dissipation at the electrode surface by reacting with HF and suppressing LiF and $\rm H_2O$ formation (reaction [1]). Therefore, the HF autocatalytic formation was suppressed (reaction [2]). [81] It has been shown that a ZnO coating multi-layer with thickness larger than 10 nm can form additional OH* sites via the reaction with HF and, thereby, OH* sites interrupted the generation of additional HF and the formation of LiF and $\rm H_2O$ were suppressed. [81] Therefore, the pitting corrosion induced by the HF attack was suppressed, as shown in **Figure 7a–c**. The thickness of the Al:ZnO coating layer is in the range of 20–40 nm (Figure S8i,j, Supporting Information).

An in-situ XRD study has shown that, for an uncoated $LiCoO_2$ electrode, the c lattice constant increased due to the Li^+ ion dissipation at high temperatures, causing a columbic repulsion between the CoO_2 layers. In the case of a $ZnO-coated\ LiCoO_2$ electrode, the Zn^{2+} ions diffused into the $LiCoO_2$ lattice at elevated

temperatures and suppressed the increase of the c lattice constant by occupying the Li⁺ free sites. [64] A model based on an in – operando XAS study of MgO-coated LiCoO₂ thin-film electrodes has shown that the Mg²⁺ ions, which diffused into the LiCoO₂ lattice during post-deposition annealing, formed a solid solution in which the Mg²⁺ ions occupied the Li⁺ free sites and behaved as pillars to stabilize the crystal structure of the electrode surface during de-lithiation. [46,88] This proposed model is also valid in the case of Al:ZnO – coated NMC-111 electrodes, since the ionic radius of the Zn²⁺ ion (0.74 Å) is smaller than that of the Li⁺ ion (0.76 Å), which is also the case for the Mg²⁺ ion (0.72 Å). [89]

3. Conclusions

In this work, the structural and chemical changes of uncoated and Al:ZnO - coated NMC -111 powder electrodes before and after electrochemical cycling in the voltage range of 3.0-4.5 V have been studied in detail using analytical TEM and XPS. During the coating process and the subsequent annealing, the Al:ZnO coating layer formed a solid solution at the surface/coating layer interface as the Zn and Al ions diffused into the electrode surface. In the case of the uncoated NMC -111 electrode after 50 cycles, due to a direct electrolyte exposure of the surface, pitting corrosion due to a HF attack and an irreversible phase transformation from a trigonal layered to a disordered rock-salt phase occurred at the electrode surface, leading to capacity fading. Moreover, Li+ and oxygen losses, cation mixing, and the reduction of the oxidation state of the Co and Mn ions occurred at the electrode surface, while no change in the oxidation state of Ni ion occurred. In the case of Al:ZnO - coated NMC-111 electrode after 50 cycles, pitting corrosion, cation mixing, and the irreversible phase transformation were mitigated, and the trigonal layered structure was preserved as the coating covered the surface of the electrode and protected it from direct electrolyte exposure. Moreover, Li+ and oxygen losses and also the reduction of the oxidation state of the Co and Mn ions did not occur, leading to an improvement in capacity retention and rate capability.

4. Experimental Section

Sample Preparation: A nano-scale Al:ZnO layer was coated onto the NMC-111 powder electrode using a microwave-assisted sol-gel synthesis method. For that, Zn (II) acetate (≥99.9%, VWR Germany) and Al (III) isopropoxide (≥99.9%, VWR Germany) were added to a 10 mL glass container in a molar ratio of 98:2. Then, the mixture was dispersed in 5 mL benzyl alcohol (99.8%, anhydrous) under an inert gas atmosphere. Afterwards, 1 g of the NMC-111 powder electrode (>99.5%, Targray) was slowly added to the reaction mixture under vigorous stirring. One sample was prepared likewise with 1 g of the NMC-111 powder electrode and 5 mL benzyl alcohol as a reference. The samples were heated up in a CEM Discover SP microwave reactor with a high stirring rate equipped with a build-in camera. Dissolution of the metal precursors occurred in the temperature range of 140-160 °C. Al:ZnO precipitation was detected in the temperature range of 160–180 °C. The samples were cleaned with diethyl ether and also with ethanol, followed by a separation via centrifugation and drying overnight at 80 °C in a vacuum furnace. The synthesis of Al:ZnO – coated NMC-111 powder electrodes and the effect of the synthesis parameters on the morphology and electrochemical performance were explained in detail in the previous paper.[58]

Characterization Methods: A morphological study was conducted using a dual-beam focused ion beam/scanning electron microscope



www.advmatinterfaces.de

(FIB/SEM ZEISS cross-beam 340) with an accelerating voltage of 5 kV. X-ray diffraction (XRD) was carried out by a Siemens D-5000 X-ray diffractometer using a Cu-K α source and the sample was rotated during the XRD acquisition. X-ray photoelectron spectroscopy (XPS) samples were transported in a sealed vessel to a glovebox connected to the spectrometer (Axis Ultra DLD, Kratos, U.K.). The sample was held in the instrument's ultra-high vacuum chamber for more than 12 h to completely remove volatile species. XPS was measured using a monochromatic Al-Klphasource (h ν = 1486.6 eV) at 10 mA emission current and an acceleration voltage of 12 kV. The pressure within the analysis chamber was equal or less than 5*10⁻⁸ mbar. A charge neutralizer was used to compensate for the charging of the sample. The measurement was carried out at 0° angle of emission. Survey spectra were recorded at a pass energy of 160 eV. For measurements of the uncoated electrode, the following core spectra were recorded at a pass energy of 20 eV: F 1s, Mn 2p, O 1s, C 1s, P 2p, and Li 1s. For the coated electrode, the Zn 2p spectrum was recorded as well. Due to low signal intensities, the Mn 2p core spectra were additionally recorded using a pass energy of 160 eV. The analysis area was \approx 700 μ m \times 300 μ m. Energy calibration was carried out with the help of Casa XPS.[90] For this, the binding energy (BE) of the measured spectra was calibrated internally by using a distinct peak in the F 1s spectra (M-F/Li-F peak at BE = 685 eV).

Electrochemical Measurement: The NMC -111 powder electrode was mixed with polyvinylidene fluoride (PVDF, VWR, Germany) and carbon black (Black Pearls) in the ratio 80:10:10 and dispersed in N-methyl-2pyrrolidone (VWR, Germany). Then the slurries were cast onto aluminum foil with an MSK-AFA-HC100 tape casting coater (MTI Corporation) and dried at 80 °C overnight. The cathodes were punched into round disks with a diameter of 1.27 cm. The coin cells were assembled using lithium foil as counter electrode and $LiPF_{6}$ - ethylene carbonate (EC)/dimethyl carbonate (DMC) (50/50) solution (Sigma-Aldrich) as electrolyte in an argon-filled glovebox (H_2O and O_2 content < 0.1 ppm). The galvanostatic charge-discharge measurements were carried out using a VMP-300 electrochemical measurement equipment (Biologic Science Instruments) at 25 °C. The cyclic stability test was performed at C/2 rate in the voltage range of 3.0 - 4.5 V. The rate capability test was performed at different C-rates (C/20, C/10, C/5, C/2) in the voltage ranges of 3.0 - 4.2 V and 3.0 - 4.5 V followed by a constant voltage step for 1 h. The specific discharge capacities were calculated according to the total mass of Al:ZnO coated NMC-111 powder electrode (4 ±0.1 mg).

Electron Microscopy: High-resolution transmission electron microscopy (HR-TEM) coupled with Fast Fourier Transform (FFT) analysis, annular bright-field scans (ABF-STEM), high-angle annular dark-field scans (HAADF-STEM), energy dispersive X-ray spectroscopy (EDX-STEM), NBD, and EELS techniques were carried out using a FEI Titan Themis G3 300 TEM equipped with a Gatan Image Filter (GIF) quantum ER/965 P dual EEL spectrometer, Ceta 16 m camera, Super-X EDX detector, HAADF, and ABF image detectors. The EELS spectra were recorded at 0.25 eV/channel and 0.1 eV/channel dispersion, and a drift corrector was used during EELS-SI acquisition. The EELS-SI was used in order to acquire the summed spectra over the selected area of an electrode. The L₃/L₂ intensity ratio was performed first by subtracting the background using a power law and then by considering a positive contribution of the second derivative of EELS spectra under individual $\rm L_2$ and $\rm L_3$ peaks. $^{[91,92]}$ The low-loss and core-loss spectra were acquired simultaneously (dual EELS mode) and the energy of EELS spectra was calibrated with respect to the zero-loss peak. The peak-to-noise ratio of EELS-SI was improved using the principal components analysis (PCA) implemented in Gatan Digital Micrograph (DM3) to acquire meaningful maps.^[93] A micro-probe mode was used for the nano-beam diffraction spectrum image (NBD-SI) acquisition with semi-convergence angle of 1.0 mrad. The accelerating voltage of 300 kV was used for the TEM measurements. The NBD-SI data processing was performed using the custom DM plug-ins.^[50,94] The EELS, HR-TEM, and NBD data, acquired from the different regions of samples, were consistent. Since the electrode materials are beam sensitive, low exposure times and low electron beam currents were used for acquiring NBD, EDX, and EELS-SI. A STEM image was acquired from the sample before and after NBD and EELS acquisition to ensure that no artifact induced by e-beam damage was observed. The cycled coin cells

in the discharged state were disassembled and the NMC-111 electrodes were recovered and washed with dimethyl carbonate (DMC) inside an Ar-filled glove box. The TEM samples of the NMC-111 electrode were prepared using a FIB/SEM ZEISS cross-beam 340. The final polishing of the TEM lamella was performed using an acceleration voltage of 5 kV to remove the possible artifact induced by the Ga-ion beam. The prepared TEM samples were stored inside a N_2 -filled glove box (H_2O and O_2 content <1 ppm). In the case of a pristine NMC-111 powder electrode, the TEM sample was prepared by dispersing the cathode powder on a carbon-supported Cu-grid inside a N_2 -filled glove box followed by a transfer to the TEM using a vacuum transfer holder (Gatan).

Supporting Information

Supporting Information is available from the Wiley Online Library or from the author.

Acknowledgements

The authors would like to acknowledge the Bundesministerium für Wirtschaft und Energie (BMWi) for funding the project "NanoBat—Nanostrukturierte Batteriematerialien" (Grant numbers: 03ET6104A and 03ET6104B). Furthermore, the authors would like to acknowledge Deutsche Forschungsgemeinschaft (DFG) for funding the TEM equipment via the Major Research Instrumentation Program under INST 211/719-1 FUGG. The authors also acknowledge the Münster Nanofabrication Facility (MNF) of the University of Münster for providing the FIB-SEM equipment and clean room facility.

Open access funding enabled and organized by Projekt DEAL.

Conflict of Interest

The authors declare no conflict of interest.

Data Availability Statement

The data that support the findings of this study are available from the corresponding author upon reasonable request.

Keywords

capacity fading, electron energy-loss spectroscopy, nano-beam electron diffraction, surface modification, transmission electron microcopy

Received: August 11, 2023 Revised: October 18, 2023 Published online: November 23, 2023

- [1] A. Manthiram, ACS Cent. Sci. 2017, 3, 1063.
- [2] Y. Ding, Z. P. Cano, A. Yu, J. Lu, Z. Chen, *Electrochem. Energy Rev.* 2019, 2, 1.
- [3] J.-M. Tarascon, M. Armand, Nature 2001, 414, 359.
- [4] N. Nitta, F. Wu, J. T. Lee, G. Yushin, Mater. Today 2015, 18, 252.
- [5] W. Li, E. M. Erickson, A. Manthiram, Nat. Energy 2020, 5, 26.
- [6] S.-T. Myung, F. Maglia, K.-J. Park, C. S. Yoon, P. Lamp, S.-J. Kim, Y.-K. Sun, ACS Energy Lett. 2017, 2, 196.
- [7] F. Schipper, E. M. Erickson, C. Erk, J.-Y. Shin, F. F. Chesneau, D. Aurbach, J. Electrochem. Soc. 2017, 164, A6220.

ADVANCED SCIENCE NEWS

www.advancedsciencenews.com

INTERFACES

*A*DVANCED

www.advmatinterfaces.de

- [8] J. Xu, F. Lin, M. M. Doeff, W. Tong, J. Mater. Chem. A 2017, 5, 874.
- [9] M. Hu, X. Pang, Z. Zhou, J. Power Sources 2013, 237, 229.
- [10] J. Deng, L. Xi, L. Wang, Z. Wang, C. Y. Chung, X. Han, H. Zhou, J. Power Sources 2012, 217, 491.
- [11] B. J. Hwang, Y. W. Tsai, D. Carlier, G. Ceder, Chem. Mater. 2003, 15,
- [12] S.-T. Myung, M.-H. Lee, S. Komaba, N. Kumagai, Y.-K. Sun, Electrochim. Acta 2005, 50, 4800.
- [13] J. C. Garcia, J. Bareño, J. Yan, G. Chen, A. Hauser, J. R. Croy, H. Iddir, J. Phys. Chem. C 2017, 121, 8290.
- [14] C. Julien, A. Mauger, K. Zaghib, H. Groult, Inorganics 2014, 2, 132.
- [15] C. Zech, M. Evertz, M. Börner, Y. Kayser, P. Hönicke, M. Winter, S. Nowak, B. Beckhoff, J. Anal. At. Spectrom. 2021, 36, 2056.
- [16] H. Liu, M. Bugnet, M. Z. Tessaro, K. J. Harris, M. J. R. Dunham, M. Jiang, G. R. Goward, G. A. Botton, *Phys. Chem. Chem. Phys.* 2016, 18, 29064.
- [17] S. Sicolo, M. Mock, M. Bianchini, K. Albe, Chem. Mater. 2020, 32, 10096.
- [18] S. Hwang, D. H. Kim, K. Y. Chung, W. Chang, Appl. Phys. Lett. 2014, 105.
- [19] S. Muto, Y. Sasano, K. Tatsumi, T. Sasaki, K. Horibuchi, Y. Takeuchi, Y. Ukyo, J. Electrochem. Soc. 2009, 156, A371.
- [20] F. Lin, I. M. Markus, D. Nordlund, T.-C. Weng, M. D. Asta, H. L. Xin, M. M. Doeff, Nat. Commun. 2014, 5, 3529.
- [21] J. Xu, E. Hu, D. Nordlund, A. Mehta, S. N. Ehrlich, X.-Q. Yang, W. Tong, ACS Appl. Mater. Interfaces 2016, 8, 31677.
- [22] J. Li, X. Wang, X. Kong, H. Yang, J. Zeng, J. Zhao, ACS Sustainable Chem. Eng. 2021, 9, 10547.
- [23] I. Nakai, K. Takahashi, Y. Shiraishi, T. Nakagome, F. Nishikawa, J. Solid State Chem. 1998, 140, 145.
- [24] A. Manthiram, J. Choi, J. Power Sources 2006, 159, 249.
- [25] H. Liu, K. J. Harris, M. Jiang, Y. Wu, G. R. Goward, G. A. Botton, ACS Nano 2018, 12, 2708.
- [26] D. P. Abraham, R. D. Twesten, M. Balasubramanian, J. Kropf, D. Fischer, J. Mcbreen, I. Petrov, K. Amine, J. Electrochem. Soc. 2003, 150, A1450
- [27] Z. Chen, Y. Qin, K. Amine, Y.-K. Sun, J. Mater. Chem. 2010, 20, 7606
- [28] L. J. Fu, H. Liu, C. Li, Y. P. Wu, E. Rahm, R. Holze, H. Q. Wu, Solid State Sci. 2006, 8, 113.
- [29] T. Li, X.-Z. Yuan, L. Zhang, D. Song, K. Shi, C. Bock, Electrochem. Energy Rev. 2020, 3, 43.
- [30] S.-T. Myung, K. Izumi, S. Komaba, Y.-K. Sun, H. Yashiro, N. Kumagai, Chem. Mater. 2005, 17, 3695.
- [31] G. Singh, R. Thomas, A. Kumar, R. S. Katiyar, A. Manivannan, J. Electrochem. Soc. 2012, 159, A470.
- [32] D. Becker, M. Börner, R. Nölle, M. Diehl, S. Klein, U. Rodehorst, R. Schmuch, M. Winter, T. Placke, ACS Appl. Mater. Interfaces 2019, 11, 18404
- [33] A. M. A. Hashem, A. E. Abdel-Ghany, A. E. Eid, J. Trottier, K. Zaghib, A. Mauger, C. M. Julien, J. Power Sources 2011, 196, 8632.
- [34] A. Yano, S. Aoyama, M. Shikano, H. Sakaebe, K. Tatsumi, Z. Ogumi, J. Electrochem. Soc. 2015, 162, A3137.
- [35] K. Araki, N. Taguchi, H. Sakaebe, K. Tatsumi, Z. Ogumi, J. Power Sources 2014, 269, 236.
- [36] H. Sclar, O. Haik, T. Menachem, J. Grinblat, N. Leifer, A. Meitav, S. Luski, D. Aurbach, J. Electrochem. Soc. 2012, 159, A228.
- [37] K. Yoo, Y. Kang, K. Im, C.-S. Kim, Materials (Basel) 2017, 10, 1.
- [38] A. M. Wise, Chem. Mater. 2015, 27, 6146.
- [39] N. Kimura, E. Seki, T. Tooyama, S. Nishimura, J. Alloys Compd. 2021, 869, 159259.
- [40] D. Mohanty, K. Dahlberg, D. M. King, L. A. David, A. S. Sefat, D. L. Wood, C. Daniel, S. Dhar, V. Mahajan, M. Lee, F. Albano, Sci. Rep. 2016, 6, 1.

- [41] X. Dai, A. Zhou, J. Xu, B. Yang, L. Wang, J. Li, J. Power Sources 2015, 298, 114.
- [42] B. Shen, P. Zuo, Q. Li, X. He, G. Yin, Y. Ma, X. Cheng, C. Du, Y. Gao, Electrochim. Acta 2017, 224, 96.
- [43] K. J. Carroll, D. Qian, C. Fell, S. Calvin, G. M. Veith, M. Chi, L. Baggetto, Y. S. Meng, Phys. Chem. Chem. Phys. 2013, 15, 11128.
- [44] K.-X. Wang, X.-H. Li, J.-S. Chen, Adv. Mater. 2015, 27, 527.
- [45] L. Dahéron, R. Dedryvère, H. Martinez, D. Flahaut, M. Ménétrier, C. Delmas, D. Gonbeau, Chem. Mater. 2009, 21, 5607.
- [46] Y. Orikasa, D. Takamatsu, K. Yamamoto, Y. Koyama, S. Mori, T. Masese, T. Mori, T. Minato, H. Tanida, T. Uruga, Z. Ogumi, Y. Uchimoto, Adv. Mater. Interfaces 2014, 1, 1.
- [47] D. Qian, C. Ma, K. L. More, Y. S. Meng, M. Chi, NPG Asia Mater 2015, 7, e193.
- [48] Z.-H. Xie, Z. Jiang, X. Zhang, J. Electrochem. Soc. 2017, 164, A2110.
- [49] L. Yu, M. Li, J. Wen, K. Amine, J. Lu, Mater. Chem. Front. 2021, 5, 5186.
- [50] C. Gammer, V. Burak Ozdol, C. H. Liebscher, A. M. Minor, *Ultramicroscopy* 2015, 155, 1.
- [51] J. Zhu, S. Sharifi-Asl, J. C. Garcia, H. H. Iddir, J. R. Croy, R. Shahbazian-Yassar, G. Chen, ACS Appl. Energy Mater. 2020, 3, 4799.
- [52] J. Zheng, P. Yan, J. Zhang, M. H. Engelhard, Z. Zhu, B. J. Polzin, S. Trask, J. Xiao, C. Wang, J. Zhang, Nano Res. 2017, 10, 4221.
- [53] H. Kuriyama, H. Saruwatari, H. Satake, A. Shima, F. Uesugi, H. Tanaka, T. Ushirogouchi, J. Power Sources 2015, 275, 99.
- [54] N. Y. Kim, T. Yim, J. H. Song, J.-S. Yu, Z. Lee, J. Power Sources 2016, 307, 641
- [55] J. Li, H. Liu, J. Xia, A. R. Cameron, M. Nie, G. A. Botton, J. R. Dahn, J. Electrochem. Soc. 2017, 164, A655.
- [56] S.-K. Jung, H. Gwon, J. Hong, K.-Y. Park, D.-H. Seo, H. Kim, J. Hyun, W. Yang, K. Kang, Adv. Energy Mater. 2014, 4, 1.
- [57] L. Zou, W. Zhao, H. Jia, J. Zheng, L. Li, D. P. Abraham, G. Chen, J. R. Croy, J.-G. Zhang, C. Wang, Chem. Mater. 2020, 32, 2884.
- [58] M. Wolff, S. Lobe, C. Dellen, S. Uhlenbruck, C. Ribeiro, X. H. Guichard, M. Niederberger, A. Makvandi, M. Peterlechner, G. Wilde, D. Fattakhova-Rohlfing, O. Guillon, Nano Sel. 2021, 2, 146.
- [59] F. Wu, J. Tian, Y. Su, J. Wang, C. Zhang, L. Bao, T. He, J. Li, S. Chen, ACS Appl. Mater. Interfaces 2015, 7, 7702.
- [60] X. Zhang, W. J. Jiang, A. Mauger, Qilu, F. Gendron, C. M. Julien, J. Power Sources 2010, 195, 1292.
- [61] P. Stadelmann, Microsc. Microanal. 2003, 9, 60.
- [62] D. Qian, B. Xu, M. Chi, Y. S. Meng, Phys. Chem. Chem. Phys. 2014, 16, 14665.
- [63] M. G. Kim, H. J. Shin, J.-H. Kim, S.-H. Park, Y.-K. Sun, J. Electrochem. Soc. 2005, 152, A1320.
- [64] T. Fang, J.-G. Duh, Surf. Coatings Technol. 2006, 201, 1886.
- [65] S. Jantrasee, P. Moontragoon, S. Pinitsoontorn, J. Semicond. 2016, 37, 092002.
- [66] L. Luo, M. D. Rossell, D. Xie, R. Erni, M. Niederberger, ACS Sustainable Chem. Eng. 2013, 1, 152.
- [67] J. Xie, N. Imanishi, A. Hirano, Y. Takeda, O. Yamamoto, X. B. Zhao, G. S. Cao, *Thin Solid Films* 2011, 519, 3373.
- [68] K. Nie, X. Sun, J. Wang, Y. Wang, W. Qi, D. Xiao, J.-N. Zhang, R. Xiao, X. Yu, H. Li, X. Huang, L. Chen, J. Power Sources 2020, 470, 228423.
- [69] H. Sun, B. Xia, W. Liu, G. Fang, J. Wu, H. Wang, R. Zhang, S. Kaneko, J. Zheng, H. Wang, D. Li, Appl. Surf. Sci. 2015, 331, 309.
- [70] S. Hwang, W. Chang, S. M. Kim, D. Su, D. H. Kim, J. Y. Lee, K. Y. Chung, E. A. Stach, Chem. Mater. 2014, 26, 1084.
- [71] H. Y. Asl, A. Manthiram, Science 2020, 369, 140.
- [72] J. Li, Z. R. Zhang, X. J. Guo, Y. Yang, Solid State Ionics 2006, 177, 1509.
- [73] P. Yan, J. Zheng, D. Lv, Y. Wei, J. Zheng, Z. Wang, S. Kuppan, J. Yu, L. Luo, D. Edwards, M. Olszta, K. Amine, J. Liu, J. Xiao, F. Pan, G. Chen, J.-G. Zhang, C.-M. Wang, Chem. Mater. 2015, 27, 5393.
- [74] A. Gao, Y. Sun, Q. Zhang, J. Zheng, X. Lu, J. Mater. Chem. A 2020, 8, 6337.

ADVANCED SCIENCE NEWS

www.advancedsciencenews.com



www.advmatinterfaces.de

- [75] M. Gu, I. Belharouak, A. Genc, Z. Wang, D. Wang, K. Amine, F. Gao, G. Zhou, S. Thevuthasan, D. R. Baer, J.-G. Zhang, N. D. Browning, J. Liu, C. Wang, *Nano Lett.* 2012, 12, 5186.
- [76] J. Y. Lee, J. Y. Kim, H. I. Cho, C. H. Lee, H. S. Kim, S. U. Lee, T. J. Prosa, D. J. Larson, T. H. Yu, J.-P. Ahn, J. Power Sources 2018, 379, 160
- [77] R. Jung, M. Metzger, F. Maglia, C. Stinner, H. A. Gasteiger, J. Electrochem. Soc. 2017, 164, A1361.
- [78] C. Liang, R. C. Longo, F. Kong, C. Zhang, Y. Nie, Y. Zheng, K. Cho, ACS Appl. Mater. Interfaces 2018, 10, 6673.
- [79] P. Verma, P. Maire, P. Novák, Electrochim. Acta 2010, 55, 6332.
- [80] K. Edström, T. Gustafsson, J. O. Thomas, Electrochim. Acta 2004, 50, 397.
- [81] J. L. Tebbe, A. M. Holder, C. B. Musgrave, ACS Appl. Mater. Interfaces 2015, 7, 24265.
- [82] M. Bettge, Y. Li, B. Sankaran, N. D. Rago, T. Spila, R. T. Haasch, I. Petrov, D. P. Abraham, J. Power Sources 2013, 233, 346.
- [83] Y.-S. Lee, J. Fluor. Chem. 2007, 128, 392.
- [84] M. Lang, M. S. D. Darma, K. Kleiner, L. Riekehr, L. Mereacre, M. Ávila Pérez, V. Liebau, H. Ehrenberg, J. Power Sources 2016, 326, 397.

- [85] B. Heidrich, M. Börner, M. Winter, P. Niehoff, J. Energy Storage 2021, 44, 103208.
- [86] H. Hemmelmann, J. K. Dinter, M. T. Elm, Adv. Mater. Interfaces 2021, 8.
- [87] Y.-Q. Lai, M. Xu, Z.-A. Zhang, C.-H. Gao, P. Wang, Z.-Y. Yu, J. Power Sources 2016, 309, 20.
- [88] K. Yamamoto, Y. Orikasa, D. Takamatsu, Y. Koyama, S. Mori, T. Masese, T. Mori, T. Minato, H. Tanida, T. Uruga, Z. Ogumi, Y. Uchimoto, Electrochemistry 2014, 82, 891.
- [89] M. Rahm, R. Hoffmann, N. W. Ashcroft, Chem. A Eur. J. 2016, 22, 14625.
- [90] N. Fairley, V. Fernandez, M. Richard-Plouet, C. Guillot-Deudon, J. Walton, E. Smith, D. Flahaut, M. Greiner, M. Biesinger, S. Tougaard, D. Morgan, J. Baltrusaitis, Appl. Surf. Sci. Adv. 2021, 5, 100112.
- [91] T. Riedl, T. Gemming, K. Wetzig, Ultramicroscopy 2006, 106, 284.
- [92] F. Cosandey, D. Su, M. Sina, N. Pereira, G. G. Amatucci, *Micron* 2012, 43, 22.
- [93] S. Lichtert, J. Verbeeck, Ultramicroscopy 2013, 125, 35.
- [94] C. Gammer, C. Mangler, C. Rentenberger, H. P. Karnthaler, Scr. Mater. 2010, 63, 312.